

Origins of shallow level and hole mobility in codoped *p*-type ZnO thin films

H. B. Ye, J. F. Kong, and W. Z. Shen^{a)}

Laboratory of Condensed Matter Spectroscopy and Opto-Electronic Physics, Department of Physics, Shanghai Jiao Tong University, 1954 Hua Shan Road, Shanghai 200030, People's Republic of China

J. L. Zhao and X. M. Li

State Key Laboratory of High Performance Ceramics and Superfine Microstructures, Shanghai Institute of Ceramics, Chinese Academy of Sciences, 1295 Ding Xi Road, Shanghai 200050, People's Republic of China

(Received 27 October 2006; accepted 31 January 2007; published online 8 March 2007)

A combination study of structural, optical, and electrical properties has been carried out on N–In codoped *p*-type ZnO thin films for the origins of shallow level and hole mobility. The observed small activation energy of ~ 20 meV for the hole concentration corresponds well to the results from photoluminescence and conductivity data, revealing the grain boundary trapping nature of the shallow level. The achieved hole mobility is mainly due to the lack of grain boundary barrier effect, and the codoping yielded weak ionized impurity scattering. The authors have also revealed the scattering and conduction mechanisms in these *p*-ZnO films. © 2007 American Institute of Physics. [DOI: 10.1063/1.2711538]

High quality *p*-ZnO films are essential to ZnO-based optoelectronic devices; however, the realization of *p*-type ZnO is rather difficult due to the self-compensation effect from native defects, such as oxygen vacancies and zinc interstitials¹ and/or extrinsic hydrogen incorporation.² Theoretical calculations have predicted that *p*-type doping in ZnO may be possible by substituting either group-I elements (Li, Na, and K) for Zn sites or group-V elements (N, P, and As) for O sites³ and by forming a complex of $\text{As}_{\text{Zn}}-2\text{V}_{\text{Zn}}$ or $\text{Sb}_{\text{Zn}}-2\text{V}_{\text{Zn}}$.⁴ Although different kinds of dopants, e.g., Li,⁵ N,^{6,7} P,⁸ As,⁹ and Sb,¹⁰ have been employed to achieve *p*-ZnO films by various growth techniques with the observed acceptor ionization energy (110–212 meV) close to the theoretical predictions, the deep acceptor levels and low solubility of the dopants will result in low carrier concentrations, making acceptor doping of ZnO very difficult.

Yamamoto and Yoshida¹¹ have proposed theoretically a codoping method for the improvement of *p*-ZnO growth by enhancing the acceptor incorporation and decreasing the acceptor binding energy. Several groups have realized the *p*-ZnO films by codoping acceptors (N) and donors (Al, Ga, or In),^{12–15} and some of them have achieved high hole mobilities. Room-temperature hole mobility of 140–167 cm^2/Vs and concentration of 10^{17} – 10^{18} cm^{-3} were obtained in N–Al (Ref. 12) and N–In (Ref. 14) codoped *p*-ZnO films prepared on Si substrates through reactive magnetron sputtering. Ultrasonic spray pyrolysis (USP) also produces N–In codoped *p*-ZnO films on Si substrates with a hole mobility of 155 cm^2/Vs and concentration of $\sim 10^{18}$ cm^{-3} .¹⁵ Why such an effective doping could be achieved in the *p*-ZnO grown by simple growth techniques and whether there is a shallow level in these codoped *p*-ZnO films are still open questions and are the topic of the present investigation.

The studied N–In codoped *p*-ZnO thin films were deposited by USP on Si (100) substrates at atmosphere.¹⁵ The atomic ratio of Zn/N/In in the precursor solution was con-

trolled to be 1:3:0.05, and the substrates were heated to 450 °C. Different doping concentrations were realized by the change of the deposition rate, and in the present study we have employed three N–In codoped *p*-ZnO thin films (s1, s2, and s3) with the doping concentration in the range of 10^{18} – 10^{19} cm^{-3} . A Philips FEI-CM200 transmission electron microscope (TEM) was used to perform the structural characterization of the ZnO films. The film composition was characterized by x-ray photoelectron spectroscopy (XPS) (Microlab MKII, Al $K\alpha$ source). Temperature-dependent Raman and photoluminescence (PL) measurements were carried out on a Jobin Yvon LabRAM HR 800UV micro-Raman system under excitation of a He–Cd laser (325 nm). Magnetic-field-dependent Hall measurements were taken in the van der Pauw configuration under an Oxford Instruments superconductive magnet. The Ohmic contacts were fabricated by alloying indium on the surface of the ZnO thin films and verified by the measured linear and symmetric current-voltage characteristics.

Figure 1(a) illustrates a high-resolution TEM (HRTEM) image of sample s3. It can be seen that, in addition to a thin native oxide layer (~ 2 nm), the polycrystalline ZnO thin film consists of crystallites, which have random *c*-axis orientation (002) with a uniform size of ~ 8 – 10 nm. Typical XPS spectra of sample s3 are presented in Fig. 1(b), which shows the effective N–In codoping in ZnO films. The peaks of N 1s (396.7 eV) and In $3d_{5/2}$ (444.9 eV) correspond to N–Zn and In–O bonds, respectively, while the In $3d_{3/2}$ peak (453.1 eV) is possibly related to In–N bond.¹⁵ As the average grain size can also be extracted by the quantitative calculation of the Raman line shape with a spatial correlation model (SCM),¹⁶ Fig. 1(c) shows the results for the ZnO A_1 [longitudinal optical (LO)] phonon mode of sample s3. We note that the SCM (dashed curve) can achieve a good fitting with an additional weak Lorentzian (dotted curve) in the low frequency side due to the disorder-activated zone edge LO phonons. The obtained correlation lengths of 8.2, 8.3, and 8.5 nm for samples s1, s2, and s3, respectively, correspond well to the grain size of ~ 8 – 10 nm from the HRTEM observation.

^{a)} Author to whom correspondence should be addressed; electronic mail: wzshen@sjtu.edu.cn

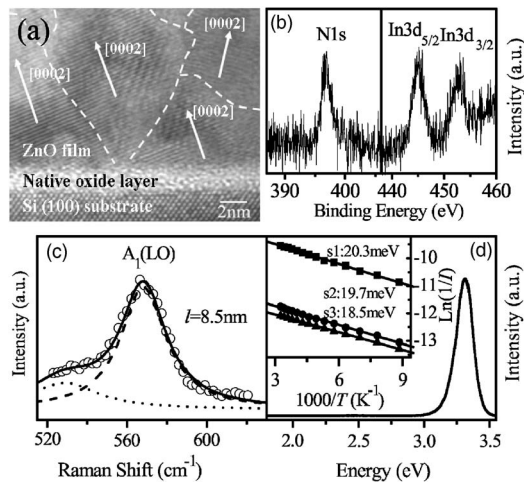


FIG. 1. (a) HRTEM image of sample s3. (b) XPS spectra of sample s3. (c) Raman spectrum (open circles) fitted by the combination (solid curve) of the SCM (dashed curve) and Lorentzian (dotted curve) for sample s3 at room temperature. (d) Room-temperature PL spectrum of sample s3, together with the integrated NBE luminescence intensity I as a function of inverse temperature T for the three N–In codoped p -ZnO thin films shown in the inset.

Room-temperature PL spectrum of sample s3, as shown in Fig. 1(d), is dominated by the near-band-edge (NBE) band, while the deep-level emission related to structural defects is almost undetectable. The strong NBE emission peak contains the band-to-band transition as well as the transition from the conduction band to a deep, neutral acceptor level (e, A^0). The inset of Fig. 1(d) displays the decay of integrated NBE luminescence intensity with temperature T from 113 to 308 K for the three N–In codoped p -ZnO thin films. The good linear fits yielded activation energies of 20.3, 19.7, and 18.5 meV for samples s1, s2, and s3, respectively.

In order to understand the origin of the low activation energy and electrical transport properties in p -ZnO, we performed temperature- and magnetic-field-dependent Hall measurements within these N–In codoped p -ZnO thin films. It is found that the measured hole concentration and mobility keep constants within the magnetic field of 0–2 T, which indicates one major hole carrier and stability of the experimental data. Generally, the grain boundary of a polycrystalline film contains a large amount of surface trapping states, which can trap free carriers from the bulk, resulting in a band bending and a depletion region near the grain boundary. Orton and Powell¹⁷ have discussed the electrical transport properties of polycrystalline semiconductors by comparing aver-

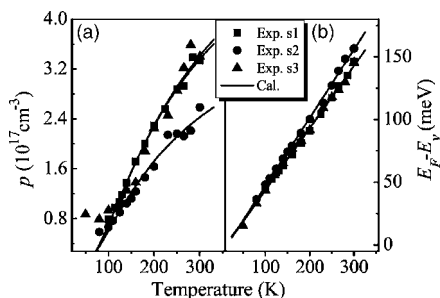


FIG. 2. (a) Temperature dependence of experimental (scatters) and calculated (solid curves) hole concentrations p for the three N–In codoped p -ZnO thin films. (b) Calculated Fermi level E_F with respect to the valence band E_v as a function of temperature from the hole concentration. The solid lines are linear fits.

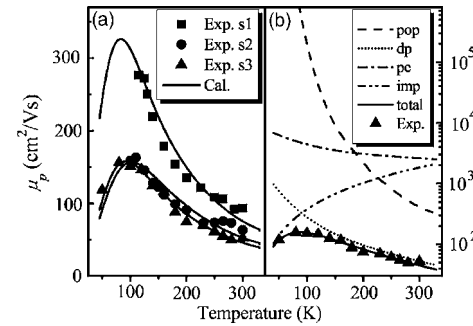


FIG. 3. (a) Temperature dependence of hole mobilities μ_p for the three N–In codoped p -ZnO thin films. (b) Experimental (filled triangles) and calculated (solid curve) hole mobility as a function of temperature for sample s3, together with the different scattering components of the mobility.

age grain size l with the Debye screening length L_D . They have concluded that, if $l > 2L_D$, a potential barrier around the grain boundary would be created, and the mobility is thermally activated while the carrier concentration varies continuously across each grain. On the other hand, if $l < 2L_D$, the band becomes flat throughout each grain, and the mobility is hardly activated thermally (though the carrier concentration may be).

We have calculated the values of L_D in p -ZnO through $L_D = (\epsilon\epsilon_0 kT / e^2 p)^{1/2}$, with ϵ the specific dielectric constant, ϵ_0 the dielectric constant in a vacuum, k the Boltzmann constant, and p the hole concentration. The obtained $2L_D$ of 12.0, 12.1, and 13.7 nm for s1, s2, and s3, respectively, satisfy the criterion of $l < 2L_D$. The bands will be effectively flat in our polycrystalline p -type ZnO thin films. We can readily calculate the hole concentration p from the charge neutrality condition of $n_t = l(N_a - N_d - n_a - p)$,¹⁷ where N_a is the acceptor doping level, N_d the donor doping level, and n_a the number of acceptors containing holes. The density of charge trapped in surface states n_t is expressed as $n_t = N_t \exp[(E_t - E_F)/kT]$, with N_t the density of grain boundary traps and E_t the grain boundary trapping level. This model can explain well the observation of the hole concentration increasing exponentially with temperature in Fig. 2(a).

The theoretical results (solid curves) in Fig. 2(a) show good agreement with the experimental data at $T > 110$ K, and the fitting results of N_a , N_t , and E_t are presented in Table I. Figure 2(b) presents the corresponding Fermi level E_F as a function of temperature, calculated from the measured hole concentration under the Boltzmann distribution. When $T < 110$ K the employment of the Boltzmann statistics for the traps is unjustified because E_F with respect to E_t is small in comparison with kT , which causes the deviation below 110 K in Fig. 2(a). The obtained N_a of 0.83×10^{19} , 1.61×10^{19} , and $5.68 \times 10^{19} \text{ cm}^{-3}$ for the three samples are in agreement with the growth design. The yielded E_t of 20.8, 18.2, and 21.2 meV correspond well to the optical activation energy from PL measurements. So we can conclude that the small (~ 20 meV) activation energy is reasonably related to this shallow grain boundary trapping level, rather than to a shallow acceptor ionization energy.

Due to the lack of the grain boundary barrier effect, relatively high hole mobilities have been observed (see Fig. 3) in these three N–In codoped p -ZnO thin films. Taking into account the scattering mechanisms due to deformation potential caused by acoustic phonon (dp), polar optical phonon (pop), piezoelectric (pe), and ionized impurity (imp), we

TABLE I. Results of fitting hole concentration and Mott's parameters for the three *p*-ZnO samples.

Samples	N_a (cm^{-3})	N_t (cm^{-2})	E_t (meV)	$N(E_F)$ ($\text{cm}^{-3} \text{eV}^{-1}$)	Diffusion (150 K)		Percolation (150 K)	
					R (nm)	W (meV)	R (nm)	W (meV)
s1	8.30×10^{18}	2.73×10^{12}	20.8	4.66×10^{19}	8.0	10.1	7.7	39.0
s2	1.61×10^{19}	1.65×10^{12}	18.2	5.00×10^{19}	7.8	10.2	7.0	49.3
s3	5.68×10^{19}	1.27×10^{12}	21.2	5.32×10^{19}	7.2	12.4	6.9	47.9

have demonstrated in Fig. 3(a) the good agreement between the theoretical mobilities (solid curves) and experimental data (scatters) using Rode's method of solving the Boltzmann transport equation.¹⁸ The detailed material parameters of ZnO in the calculations can be found elsewhere.¹⁹ Figure 3(b) displays the different scattering components of the theoretical mobility for sample s3. It is clear that the acoustic phonon scattering is the most important mechanism limiting the hole mobility at $T > 90$ K, while the ionized impurity scattering becomes dominant at $T < 90$ K.

Usually, due to the self-compensation effect and the low solubility of the acceptor dopants in ZnO, high acceptor doping seemingly becomes necessary to obtain *p*-ZnO. However, too high bulk doping will cause relatively high depletion barriers at grain boundaries. Another reason limiting hole mobility in polycrystalline ZnO films is the trap density. The grains with too high trap densities can be almost fully depleted of free carriers, leading to very high film resistivity. The N–In codoping method effectively increases the solubility of nitrogen,¹¹ resulting in few intrinsic defects in ZnO. With little grain boundary barrier effect and weak ionized impurity scattering, relatively high mobility can be achieved in the present polycrystalline *p*-ZnO thin films under moderate doping level and grain boundary trap density.

Furthermore, the dark conductivity measurements can provide further evidence for the assignment of the activation energy, in addition to the understanding of the conduction mechanism. Figure 4(a) plots the temperature dependence of conductivity σ for the three N–In codoped *p*-ZnO thin films, exhibiting two different regimes. At high temperature of 160–300 K, a good linear relationship between $\ln \sigma T$ and $1/T$ is achieved, which reveals that the nearest-neighbor hopping is the dominant conduction mechanism.²⁰ The yielded activation energies ε_A of 20.0, 23.6, and 22.8 meV for the *p*-ZnO films s1, s2, and s3, respectively, are really in good agreement with the shallow grain boundary trapping level.

Below 160 K, all the samples deviate from the $\ln \sigma T - 1/T$ linearity and display a linear relationship between

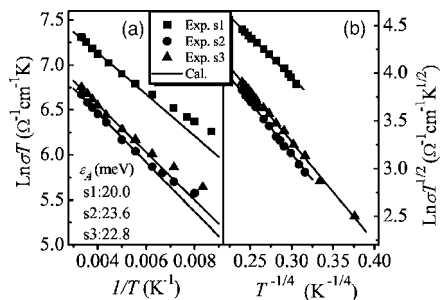


FIG. 4. (a) Plots of $\ln \sigma T$ vs $1/T$ for the three N–In codoped *p*-ZnO thin films. (b) Plots of $\ln \sigma T^{1/2}$ vs $T^{-1/4}$ for the three samples. The solid lines are the fits obtained from the VRH conduction model.

$\ln \sigma T^{1/2}$ and $T^{-1/4}$, as shown in Fig. 4(b). This kind of behavior is consistent with a variable-range hopping (VRH) mechanism.²¹ The yielded localized density of states at the Fermi level $N(E_F)$, as listed in Table I, is similar to that of Al-doped ZnO films.²² Two other Mott parameters, i.e., the hopping distance R and average hopping energy W , were calculated from the diffusion model²¹ and percolation theory. The R values are almost the same and within the range of average grain size, but the W values are quite different. According to Mott's criterion of $W \gg kT$, we conclude that the hole transport takes place along percolation paths formed by crystalline regions and the hypothesis of the diffusion model, i.e., a constant density of state distribution near the Fermi level, is not appropriate in the present *p*-ZnO samples.

This work was supported in part by the National Natural Science Foundation of China and the National Minister of Education Program for Changjiang Scholars and Innovative Research Team in University (PCSIRT).

- ¹S. B. Zhang, S. H. Wei, and A. Zunger, Phys. Rev. B **63**, 075205 (2001).
- ²C. G. Van de Walle, Phys. Rev. Lett. **85**, 1012 (2000).
- ³C. H. Park, S. B. Zhang, and S. H. Wei, Phys. Rev. B **66**, 073202 (2002).
- ⁴S. Limpijumngong, S. B. Zhang, S. H. Wei, and C. H. Park, Phys. Rev. Lett. **92**, 155504 (2004).
- ⁵Y. J. Zeng, Z. Z. Ye, W. Z. Xu, D. Y. Li, J. G. Lu, L. P. Zhu, and B. H. Zhao, Appl. Phys. Lett. **88**, 062107 (2006).
- ⁶D. C. Look, D. C. Reynolds, C. W. Litton, R. L. Jones, D. B. Eason, and G. Cantwell, Appl. Phys. Lett. **81**, 1830 (2002).
- ⁷A. Tsukazaki, A. Ohtomo, T. Onuma, M. Ohtani, T. Makino, M. Sumiya, K. Ohtani, S. F. Chichibu, S. Fuke, Y. Segawa, H. Ohno, H. Koinuma, and M. Kawasaki, Nat. Mater. **4**, 42 (2005).
- ⁸F. X. Xiu, Z. Yang, L. J. Mandalapu, J. L. Liu, and W. P. Beyermann, Appl. Phys. Lett. **88**, 052106 (2006).
- ⁹D. C. Look, G. M. Renlund, R. H. Burgener, II, and J. R. Sizelove, Appl. Phys. Lett. **85**, 5269 (2004).
- ¹⁰O. Lopatiuk-Tirpak, W. V. Schoenfeld, L. Chernyak, F. X. Xiu, J. L. Liu, S. Jang, F. Ren, S. J. Pearton, A. Osinsky, and P. Chow, Appl. Phys. Lett. **88**, 202110 (2006).
- ¹¹T. Yamamoto and H. Yoshida, Jpn. J. Appl. Phys., Part 2 **38**, L166 (1999).
- ¹²F. Zhuge, L. P. Zhu, Z. Z. Ye, D. W. Ma, J. G. Lu, J. Y. Huang, F. Z. Wang, Z. G. Ji, and S. B. Zhang, Appl. Phys. Lett. **87**, 092103 (2005).
- ¹³M. Joseph, H. Tabata, and T. Kawai, Jpn. J. Appl. Phys., Part 2 **38**, L1205 (1999).
- ¹⁴L. L. Chen, J. G. Lu, Z. Z. Ye, Y. M. Lin, B. H. Zhao, Y. M. Ye, J. S. Li, and L. P. Zhu, Appl. Phys. Lett. **87**, 252106 (2005).
- ¹⁵J. M. Bian, X. M. Li, X. D. Gao, W. D. Yu, and L. D. Chen, Appl. Phys. Lett. **84**, 541 (2004).
- ¹⁶I. H. Campbell and P. M. Fauchet, Solid State Commun. **58**, 739 (1986).
- ¹⁷J. W. Orton and M. J. Powell, Rep. Prog. Phys. **43**, 1263 (1980).
- ¹⁸D. L. Rode, Semicond. Semimetals **10**, 1 (1975).
- ¹⁹T. Makino, A. Tsukazaki, A. Ohtomo, M. Kawasaki, and H. Koinuma, Jpn. J. Appl. Phys., Part 1 **45**, 6346 (2006).
- ²⁰R. Mansfield, in *Hopping Transport in Solids*, edited by M. Pollak and B. I. Shklovshii (North-Holland, Amsterdam, 1991), p. 349.
- ²¹N. F. Mott, Adv. Phys. **16**, 49 (1967); Philos. Mag. **19**, 835 (1969).
- ²²S. Bandyopadhyay, G. K. Paul, R. Roy, S. K. Sen, and S. Sen, Mater. Chem. Phys. **74**, 83 (2002).